Supporting Information

All-Material Crosslinked Solid Polymer Electrolytes for High-Performance and Flexible Lithium Metal Battery

*Sung Yeon Bae[#], Seoyeon Kim[#], Young Ho Yoo[#], Jin-Seo Kim, Jieun Lee, Jinhan Cho, Bongjun Yeom, Jeong Gon Son**

S. Y. Bae, S. Kim, Y. H. Yoo, J.-S. Kim, J. Cho, J. G. Son
Electronic and Hybrid Materials Research Center, Korea Institute of Science and Technology
Seoul 02792, Republic of Korea
E-mail: jgson@kist.re.kr

S. Y. Bae, S. Kim, Y. H. Yoo, J. Cho, J. G. Son
KU-KIST Graduate School of Converging Science and Technology, Korea University
Seoul 02841, Republic of Korea

J. Lee
Energy Storage Research Center, Korea Institute of Science and Technology
Seoul 02792, Republic of Korea

J. Cho
Department of Chemical and Biological Engineering, Korea University
Seoul 02841, Republic of Korea

J.-S. Kim, B. Yeom
Department of Chemical Engineering, Hanyang University
Seoul 04763, Republic of Korea

[#]These authors are equally contributed.

Experimental Methods

Materials. Poly(vinylidene fluoride-co-hexafluoropropylene) (PVDF-HFP, average M_w ~ 400,000, pellets), Dimethyl carbonate (DMC) was purchased from Sigma-Aldrich. Lithium bis(trifluoromethanesulfonyl)imide (LiTFSI), 1-Ethyl-3-methylimidazolium bis(trifluoromethylsulfonyl)imide (EMIMTFSI), 2,6-bis(4-azidobenzylidene)cyclohexanone, 4-Fluoro-1,3-dioxolan-2-one (FEC) and succinonitrile was purchased from Tokyo Chemical Industry Co., Ltd. 1.0 M $LiPF_6$ in EC/DEC (1:1 vol%) with 7.5 wt% FEC electrolyte was obtained from Wellcos Co. Ltd. LiFePO4 (LFP, RD2121900A, Aleees Co., Ltd.) and lithium nickel cobalt manganese oxide (NCM811, Ossila, M2405A1) particles were used for the active materials of the cathode. Single-walled carbon nanotubes (eDIPS EC1.5) with 90 % purity and 1-3 nm diameter were purchased from Meijo Nano Carbon Inc. Lithium foil with 0.3 mm thickness was obtained from MTI Korea Co. Ltd. Poly(vinylidene fluoride) (PVDF, average Mw ~ 534,000, powder) was purchased from Sigma-Aldrich. N-Methyl-2-Pyrrolidone (NMP) was ordered from Daejung Chemical Co. Ltd. All the chemicals were used without any treatment.

Preparation of electrolytes and cell assembly. Firstly, an 8 wt% PVDF-HFP solution was prepared by vigorous magnetic stirring until PVDF-HFP pellets were fully dissolved in DMC. LiTFSI and succinonitrile (SN) were then added and stirred for an additional 2 hours. Subsequently, an ionic liquid, fluoroethylene carbonate (FEC), and a diazide-based crosslinker were introduced, followed by further stirring for 2 hours to ensure complete homogenization of the solution. The mass ratio of PVDF-HFP : IL : SN : LiTFSI was set to 1:1.5:3:0.6, while FEC was added at 5 wt% relative to the total mass of plasticizers and the diazide crosslinker was added at 1 wt% relative to the mass of solid contents(PVDF-HFP and succinonitrile). The

prepared solution was cast on electrodes, LFP cathodes and lithium metal anodes, using a 100-μm-gap doctor blade. (For the freestanding electrolytes, the solution was cast on a glass plate.) After the solvent has evaporated, the solid electrolyte film coated on the electrode (or glass plate) is exposed to UV light for 120 s. (365 nm, ~0.7 $W \cdot cm^{-2}$, UV LED spot curing system, LIIM TECH CO., LTD) After UV curing, the cell was assembled with the electrolyte-coated parts of the electrodes facing each other. (CR2032 coil cell, 20 mm diameter, 3.2 mm height, purchased from Welcos Corp.) During the cell assembly process, the conventional coin cell assembly sequence is followed without a separator. This results in a structure where the electrolytes of the two electrodes are in direct contact. Subsequently, the cell is assembled by applying a pressure using a punching machine. (Hydraulic Crimper for All Types of Coin Cells with 100 Pcs CR2032 Case – MSK – 110).

Electrode preparation. LFP cathode was prepared using a slurry casting method. Active material, SWCNT as a conductive additive and polyvinylidene fluoride were dissolved in N-methyl-2-pyrrolidone with a weight ratio of 9:0.5:0.5 to make a slurry and then coated onto 006E current collector of aluminum foil using a doctor blade (TMAX Adjustable Film Applicator 100 mm Film Casting Doctor Blade). When slurry casting, the setting thickness is 500 μm, and after drying, the final electrode active material thickness is 30 μm. The cathodes were dried in a vacuum oven at 60 °C for 24 h. The electrodes are punched to 16 mm diameter using handy punching machine. (Hand Operated Punching Tool for Electrode, Separator (WC-H125), from Welcos Corp.) The active loading density of the LFP cathode was 1.5 mg cm^{-2}.

The preparation of the pouch cell. Firstly, the cathode (NCM or LFP, as appropriate) was coated on aluminium foil. Subsequently, the electrolyte was coated on both the cathode and the lithium metal, and then dried for 12 hr. The coated lithium metal was cut to dimensions of 4.2 cm x 3.2 cm, while the anode was cut to dimensions of 4 cm x 3 cm. Aluminium lead tabs were

attached to the anode, while nickel/copper lead tabs (from Welcos Corp) were attached to the lithium metal. These components were then assembled, covered with PET film, and the pouch cell was sealed using a heat sealer (MS300, Masic Seal).

Material characterization. Field-emission scanning electron microscopy (FE-SEM, Carl Zeiss, Sigma 300) was utilized to investigate the lithium metal surface morphology at 1.0 kV. Cells that had completed their cycles were disassembled in the glove box, and residual reaction products were removed by washing with DMC organic solvent and then dried gently at room temperature prior to analysis. Mechanical tensile-stress and interfacial adhesion-strength measurements were carried out using a universal testing machine (Instron, 5900 Series Universal Testing Systems). For the stress-strain curve analysis, film-type samples with a thickness of approximately 200 μm were prepared by cutting them into dimensions of 3.0 cm x 1.5 cm, at a speed of 30 mm min^{-1}. And for the stress-strain curve of the cycle test, a speed of 15 mm min^{-1} was applied. For 180° peel test for measuring adhesion strength, after preparing the electrolyte on the Cu foil, the Cu foil and the electrolyte were pulled at a constant rate of 100 mm min^{-1}. Fourier transform infrared spectra (FT-IR) were collected over the range of 650-4000 cm^{-1} on a film-type SPE with a thickness of ~ 100 μm (3 MIR FT-IR Spectrometer, PerkinElmer, USA). Differential scanning calorimetry (DSC, DSC 4000, PerkinElmer, USA) analyzed under nitrogen gas, through temperature sweep from – 70 ℃ to 100 ℃, and from -50 ℃ to 200 ℃, at a rate of 5 ℃ min^{-1} using samples with a mass in the range of 5 – 10 mg. Battery cells were assembled inside an argon-filled glove box (Korea Kiyon Ltd.). Battery testing was carried out with a 40-channel battery cycler (WonAtech, WBCS3000S).

Electrochemical properties. The electrochemical performances of the cells were tested with 2032-type coin cells assembled using Li foil as the anode in an argon-filled glovebox (Korea Kiyon Ltd., O_2 and H_2O < 0.1 ppm). Electrochemical impedance spectroscopy (EIS) was

performed by Autolab (Metrohm, Swiss) electrochemical workstation. Measuring ionic conductivity, the AC frequency ranged from 0.1 Hz to 10^6 Hz with 5 mV potential amplitude. The ionic conductivity of the electrolytes was calculated according to Eq. (1) below:

$$\sigma = \frac{D}{R_b S} \quad (1)$$

σ represents ionic conductivity. D, R_b, S is respectively the distance between two stainless steel electrodes, bulk resistance, the contact area between the SPE and the electrodes. R_b was obtained from the fitting model of Nyquist plot. Electrochemical stability window (ESW) of the electrolytes was obtained by linear sweep voltammetry (LSV) at room temperature. Measuring cell was assembled by putting the free-standing polymer film between a stainless-steel disk and the lithium metal. Voltage scanned from -1 V to 6 V versus Li/Li^+ at a rate of 1.0 mV s^{-1}. Lithium-ion transference number (t_{Li^+}) of the electrolytes was measured by Bruce-Vincent method, with modification of considering change in the resistance of the electrolyte itself during the procedure. To a measuring cell assembled with stainless-steel electrodes, 10 mV potential (ΔV) applied to collect the current value of the initial state (I_0) and the steady-state (I_{SS}). Interfacial resistance of the initial state (R_i) and the steady state (R_{ss}) also collected by EIS with applying 5 mV AC amplitude between 10^5 Hz and 10^{-1} Hz. The value was calculated using the Eq. (2) below:

$$t_{Li^+} = \frac{I_{ss}(\Delta V - I_0 R_0)}{I_0(\Delta V - I_{ss} R_{ss})} \quad (2)$$

The cycling test of the cells was performed in the voltage range of 2.0 – 3.8 V for LFP and 2.5 – 4.2 V for NCM 811, with an initialization cycle at 0.05 C before cycling. During the test, the temperature was maintained at 20 ℃.

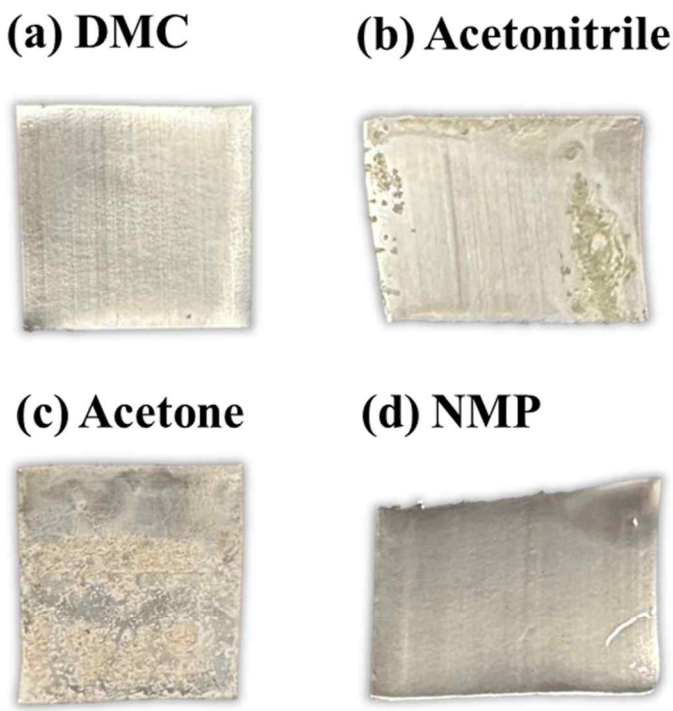

Figure S1. Photographic images of lithium foils after being directly dropped with (a) dimethyl carbonate (DMC), (b) acetonitrile, (c) acetone and (d) NMP.

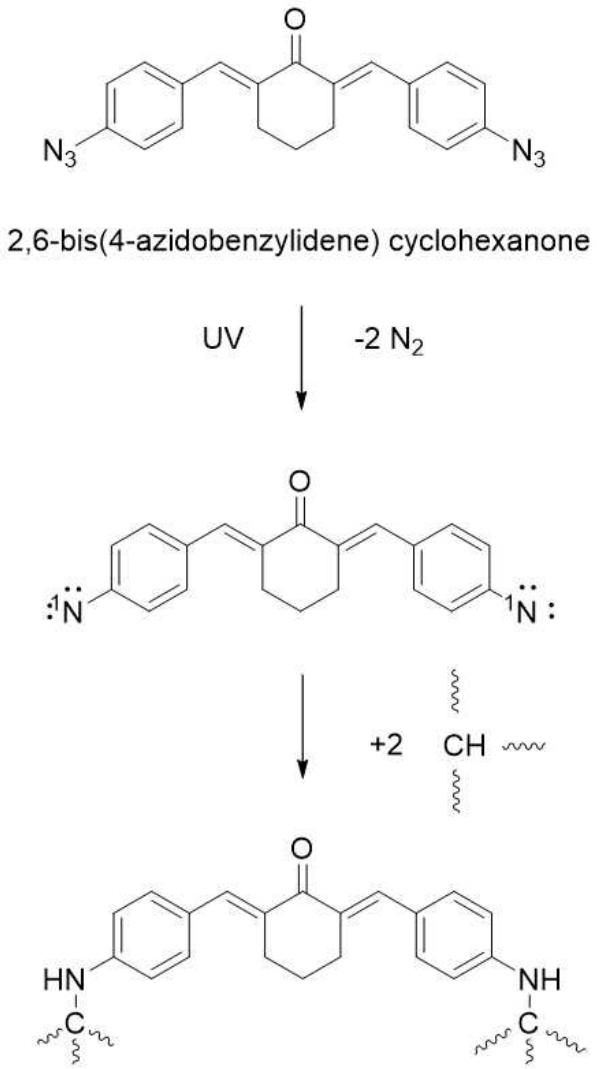

Figure S2. UV crosslinking mechanism of diazides capable of all-material curing via C-H insertion.

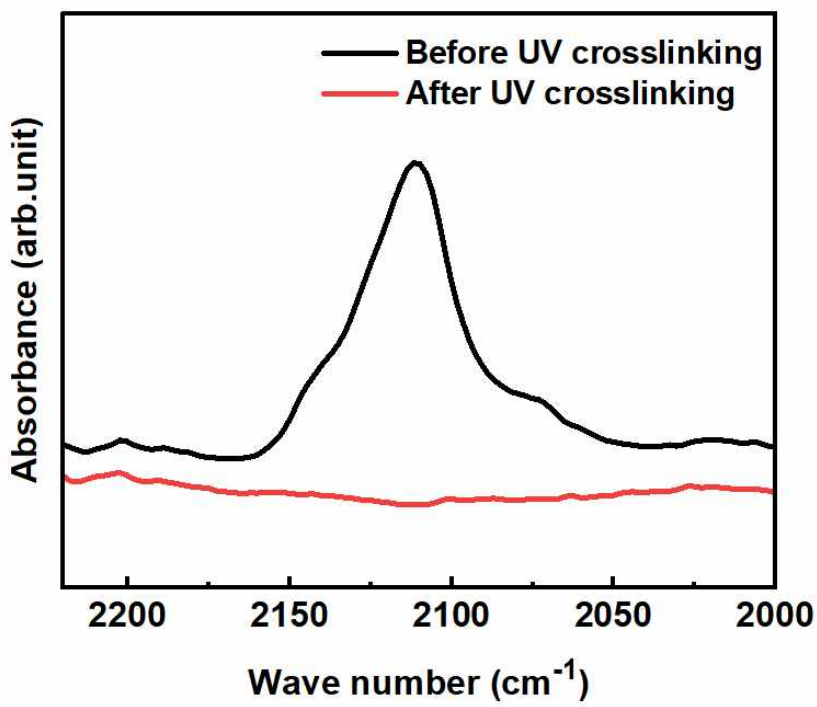

Figure S3. Photo-activation efficiency analysis of diazide crosslinker and SPE. FT-IR spectra of SPE films before (black) versus after (red) UV exposure (365 nm, 0.7 $mWcm^{-2}$, 2 min)

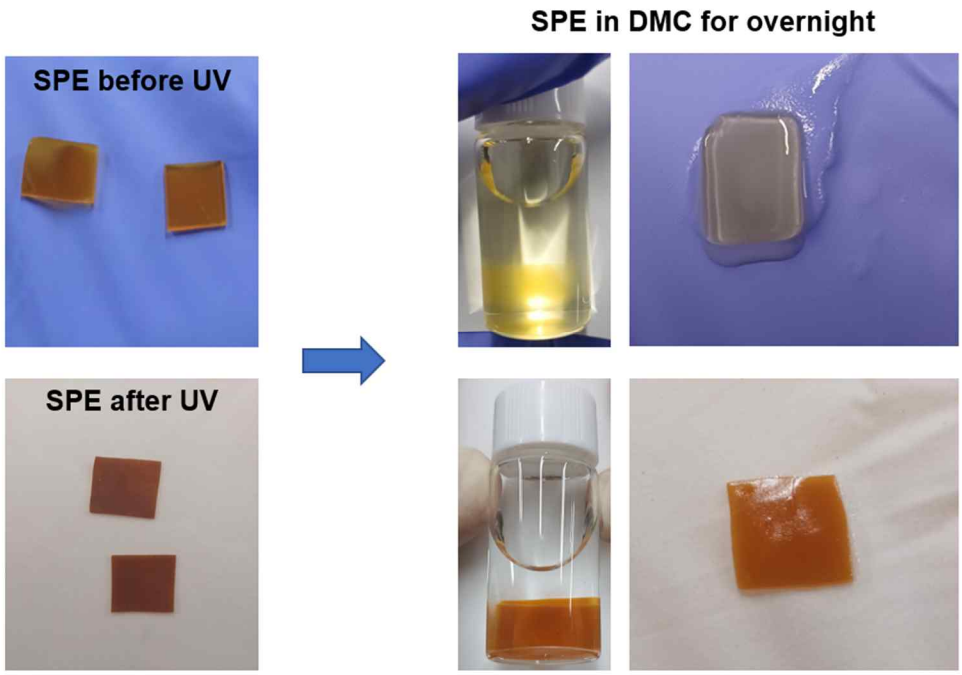

Figure S4. Solvent resistance of SPEs with and without UV curing

.

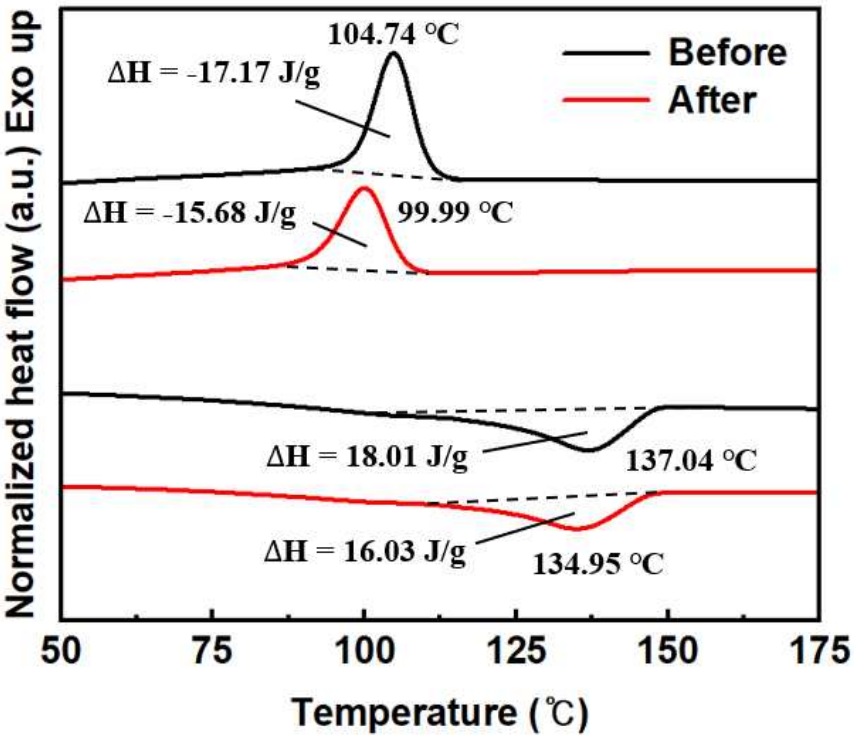

Figure S5. DSC thermograms for the PVDF-HFP and UV crosslinker composites before and after UV crosslinking. Crystallinity decreased from 44.08 % to 39.23 % after UV crosslinking.

Figure S6. Photographic image of universal testing machine (UTM) measurement of the SPEs.

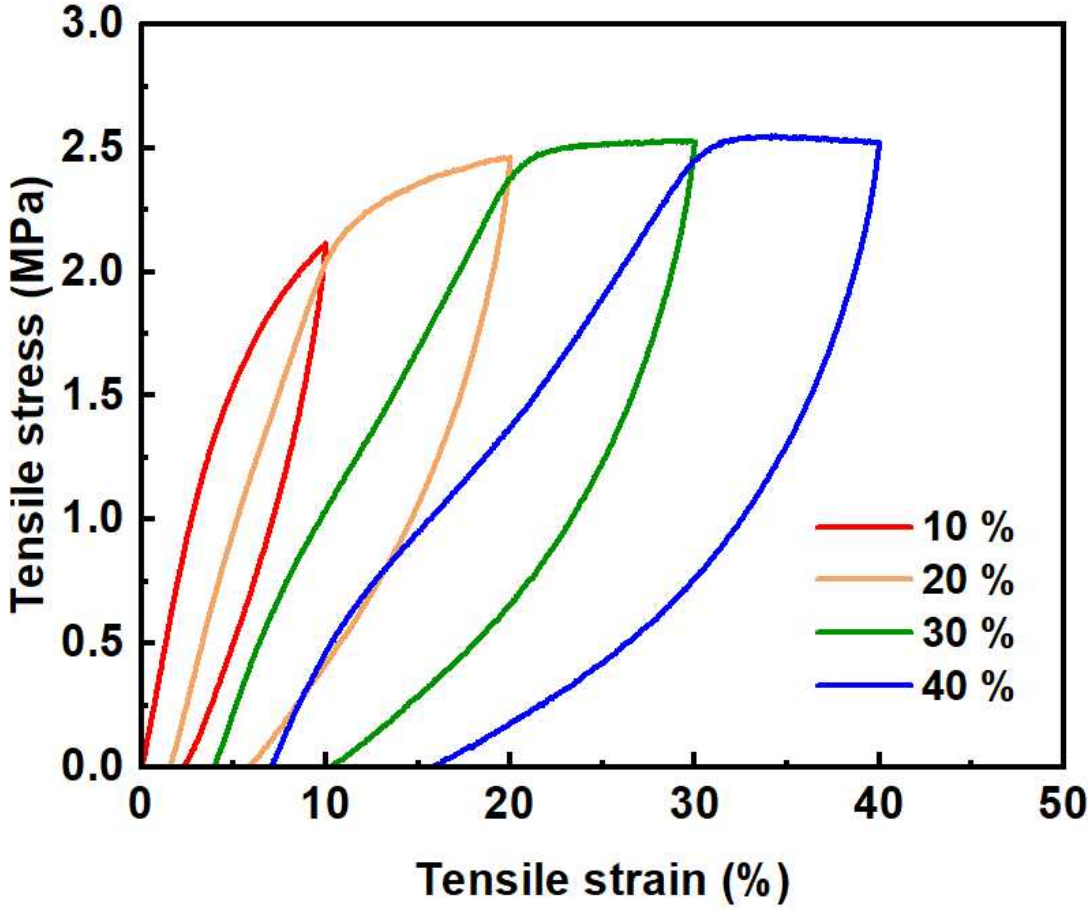

Figure S7. Cyclic stress-strain curves from repeatedly applying loading and unloading to the SPE while gradually increasing the uniaxial strain from 10% to 40%.

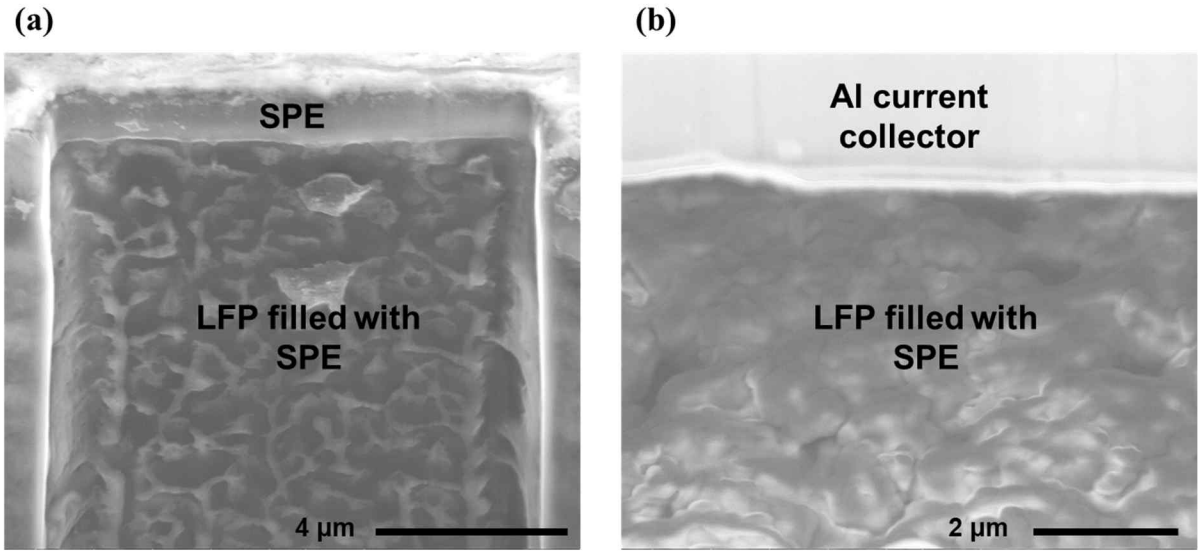

Figure S8. Cross-sectional SEM image of directly coated SPE on a porous LFP cathode prepared by focused ion beam (FIB) milling.

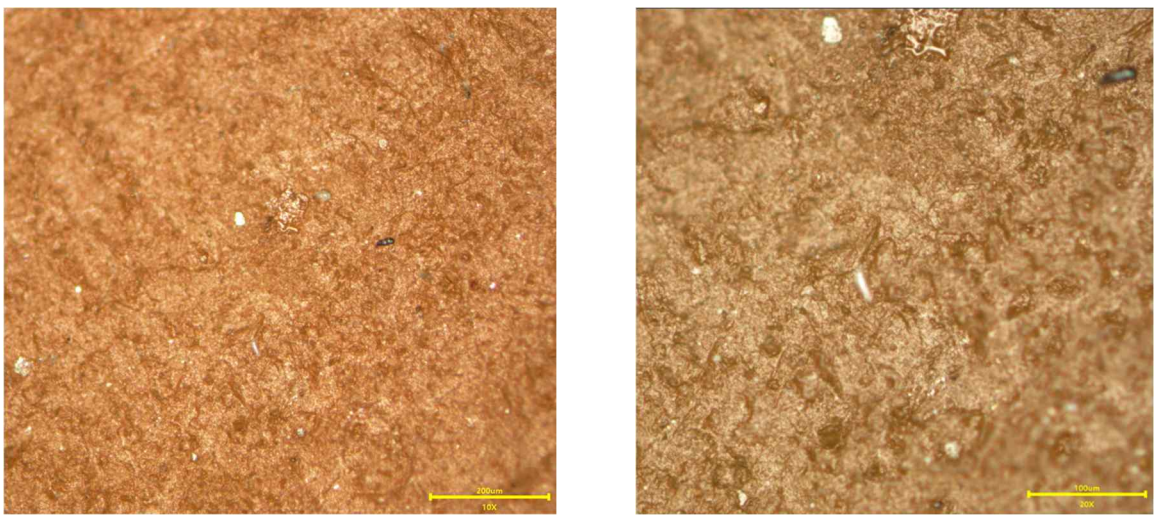

Figure S9. Top-view OM image of the SPE.

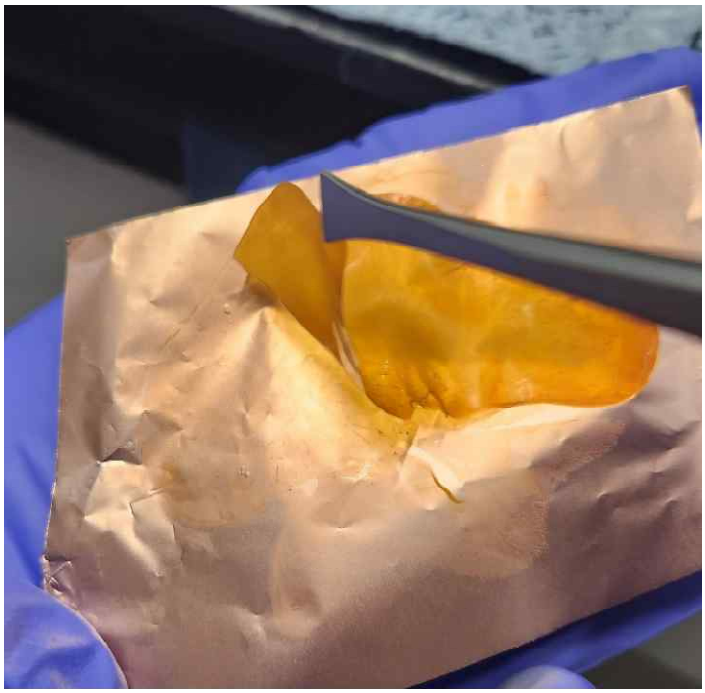

Figure S10. Peel test of the freestanding SPE: It easily separates from the Cu foil, making it impossible to perform a 180° peel-off test.

Figure S11. Photographic image of directly coated SPE with UV-crosslinking on lithium metal foil after 180° peel-off test.

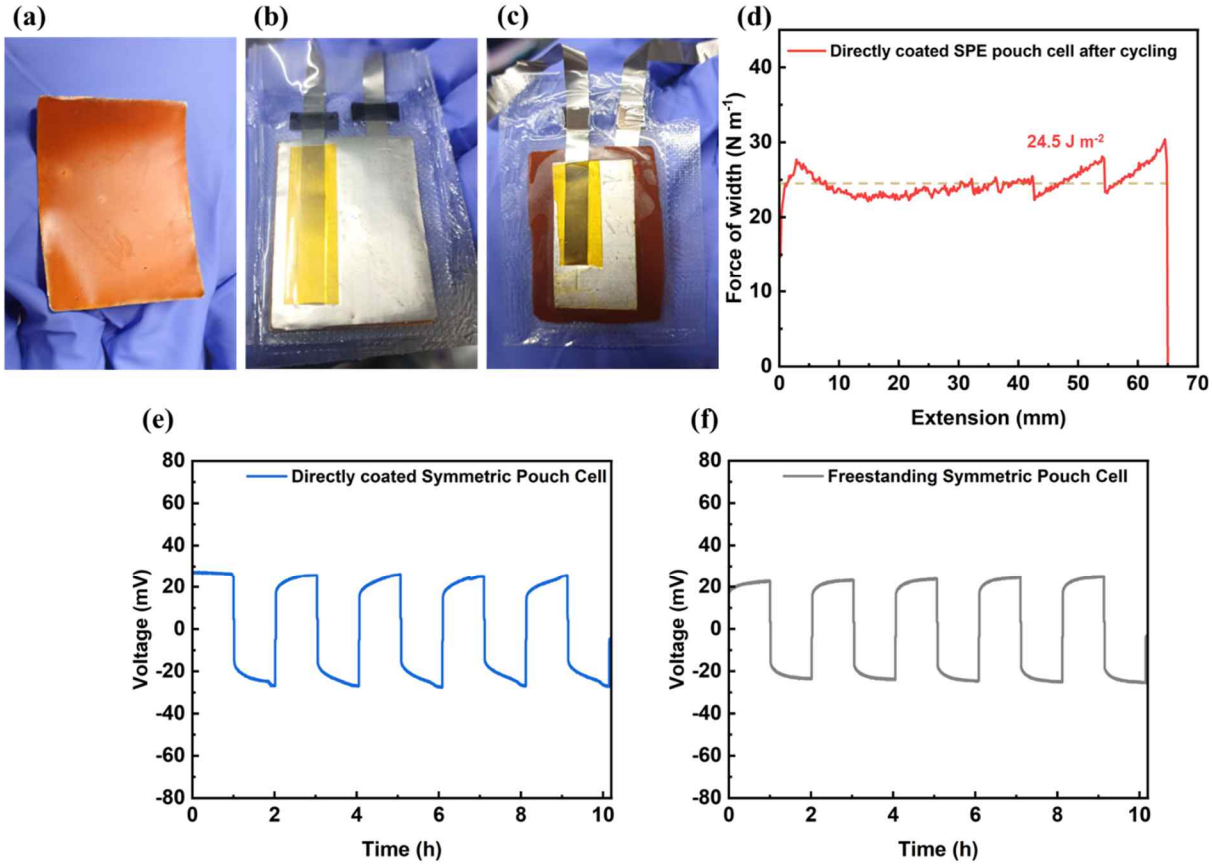

Figure S12. Photographic images of (a) conformally coated SPE on lithium metal after UV-crosslinking, (b) directly coated SPE symmetric Li//Li pouch cell (3cm × 4cm), (c) freestanding SPE symmetric Li//Li pouch cell (1.6cm × 3cm). (d) 180° peel tests between the lithium metal foil and the directly coated SPE of the lithium symmetric pouch cell after 5 charging-discharging cycles. Cycling performance of the (e) directly coated SPE (f) freestanding SPE lithium symmetric pouch cell at 0.1 mA·cm^{-2} and 0.1 mAh·cm^{-2} for 5 cycles.

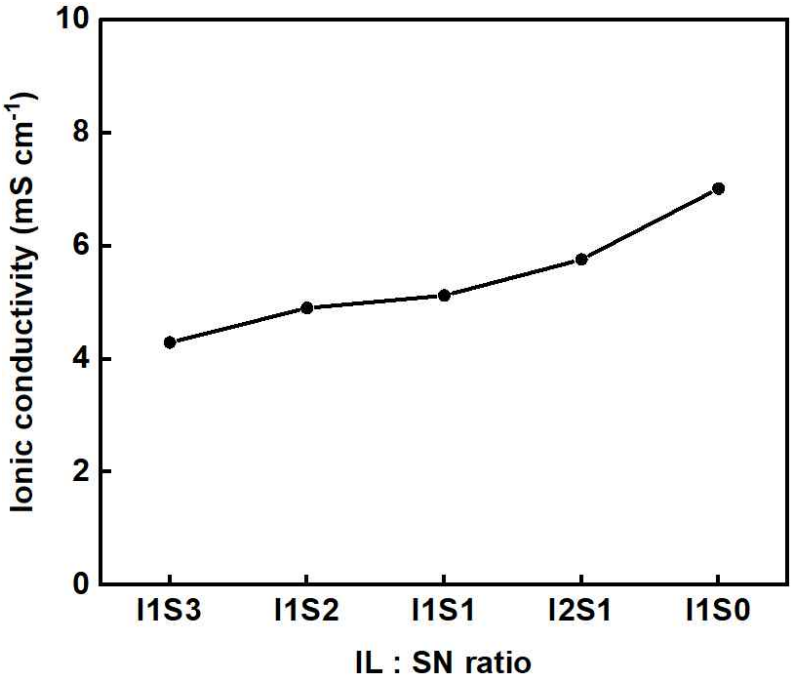

Ionic liquid : Succinonitrile	1:3	1:2	1:1	2:1	1:0
Ionic conductivity ($mScm^{-1}$)	4.29	4.90	5.12	5.76	7.02

Figure S13. Ionic conductivity according to the ratio of ionic liquid and succinonitrile at 30 ℃. The 'IxSy' notation on the graph means 'Ionic liquid (EMIMTFSI) : Succinonitrile = x : y (wt%)'

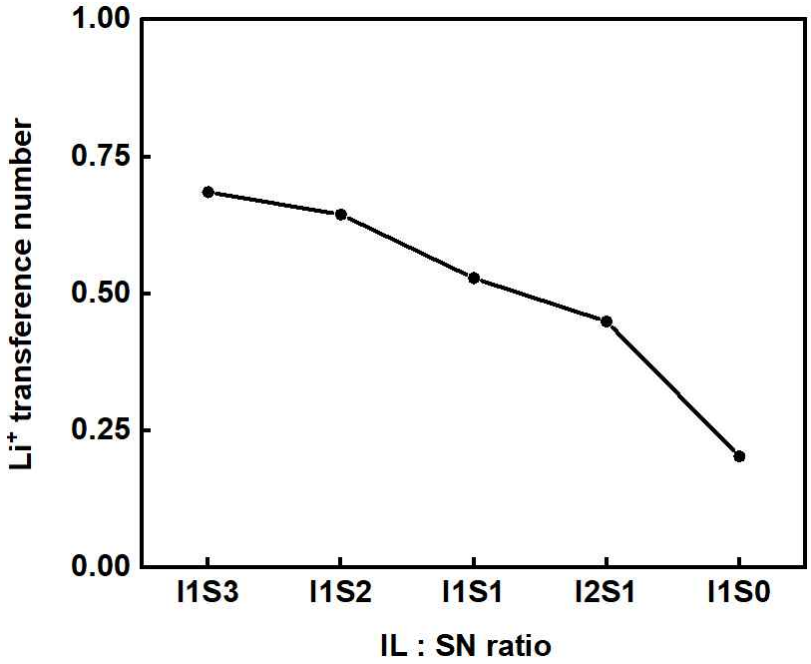

Ionic liquid : Succinonitrile	1:3	1:2	1:1	2:1	1:0
Li^+ transference number	0.686	0.644	0.528	0.449	0.203

Figure S14. Lithium ion transference number according to the ratio of ionic liquid and succinonitrile at 30 ℃.

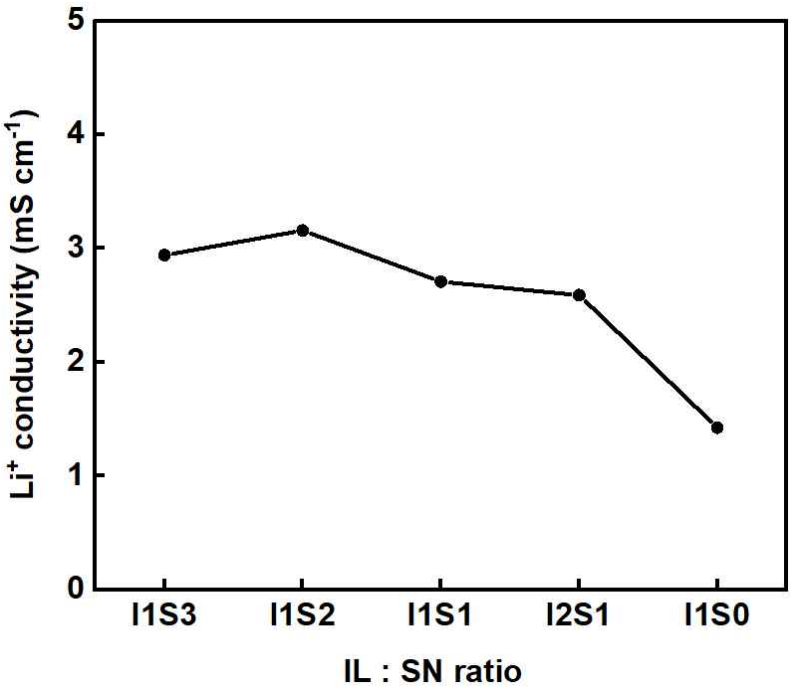

Ionic liquid : Succinonitrile	1:3	1:2	1:1	2:1	1:0
Li^+ conductivity ($mScm^{-1}$)	2.94	3.16	2.71	2.59	1.42

Figure S15. Lithium ion conductivity according to the ratio of ionic liquid and succinonitrile at 30 ℃.

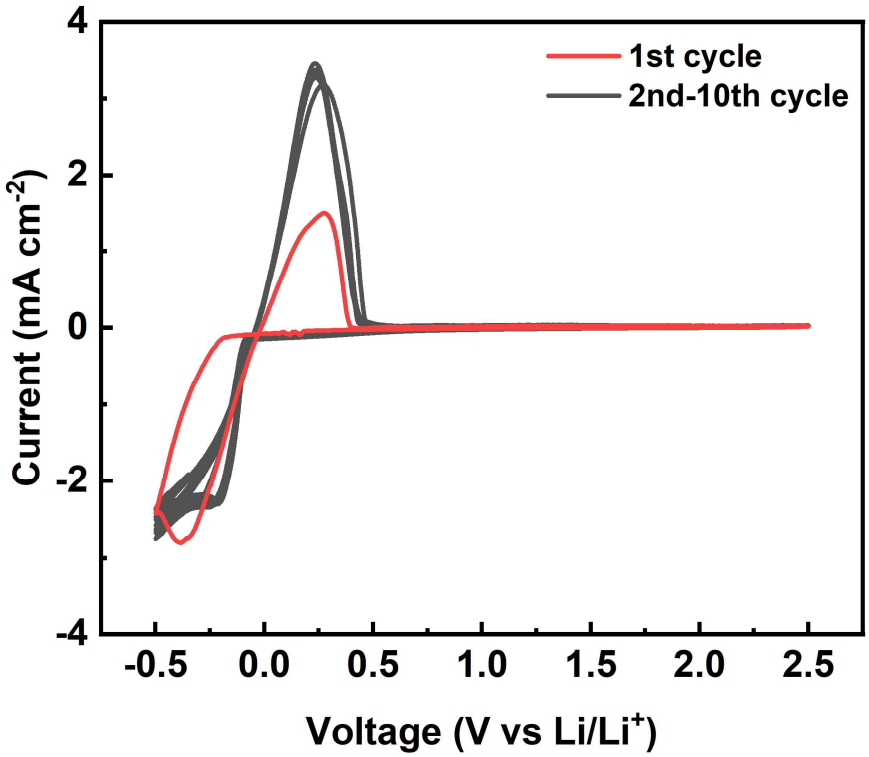

Figure S16. Cyclic voltammetry (CV) profile of the SPE for measuring electrochemical stability window.

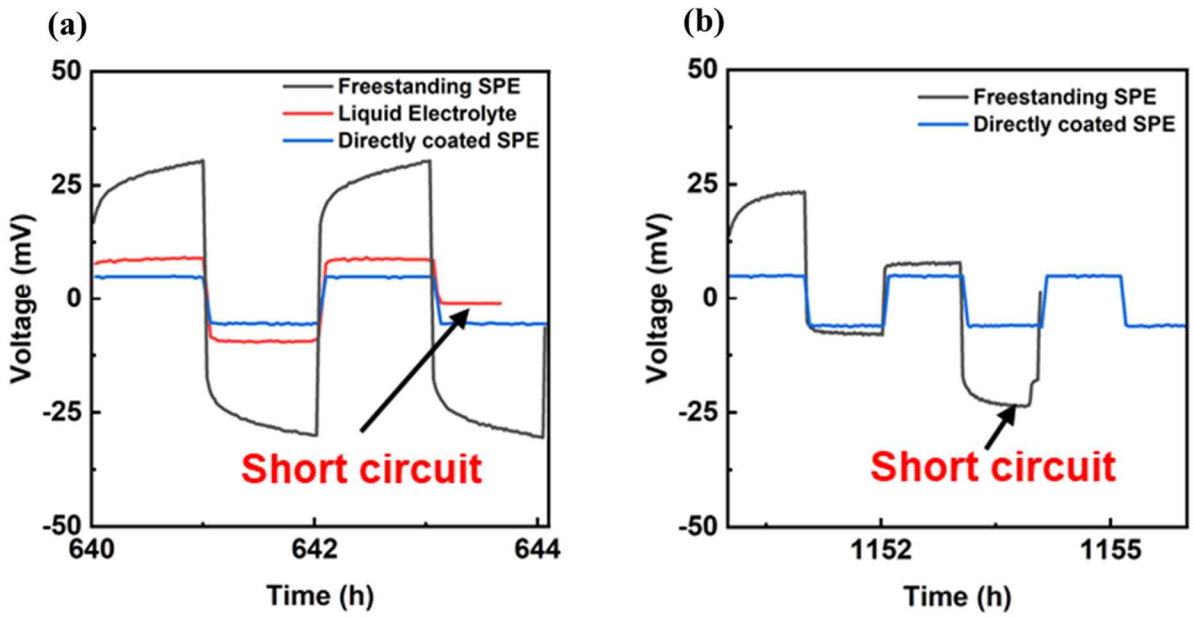

Figure S17. Enlarged voltage profiles of the cycling performance of Li symmetric cells with liquid electrolyte and solid polymer electrolyte (SPE) in free-standing and direct coating configurations at 0.1 mA·cm^{-2} and 0.1 mAh·cm^{-2}.

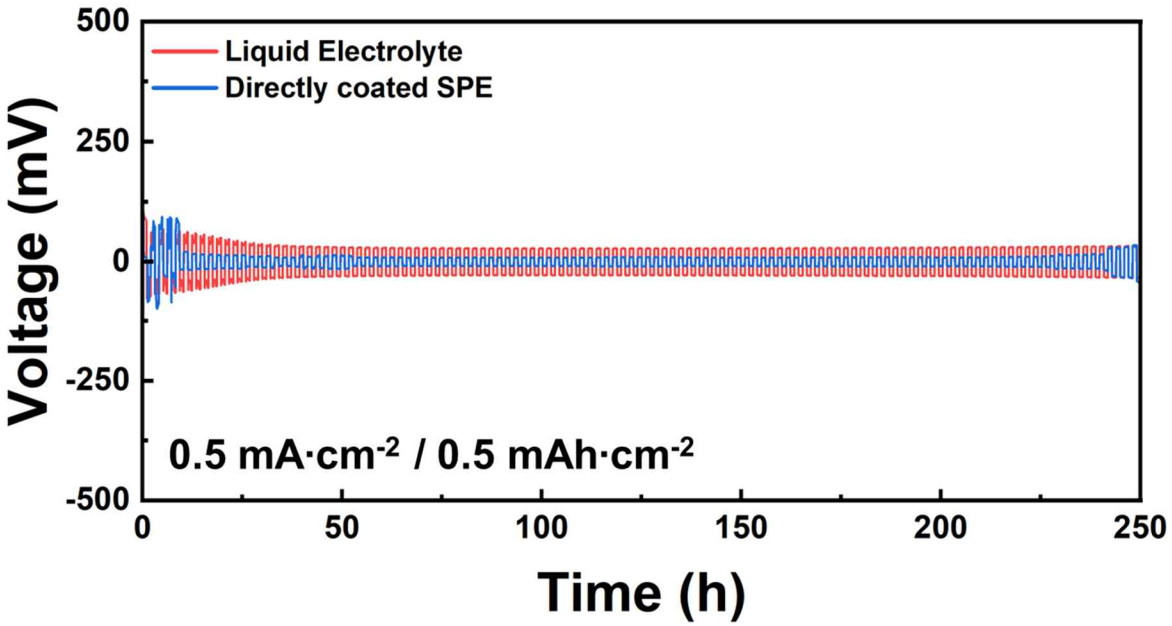

Figure S18. The cycling performance of the our-SPE Li symmetric cells with liquid electrolyte and direct coating configurations at 0.5 mA·cm^{-2} and 0.5 mAh·cm^{-2}.

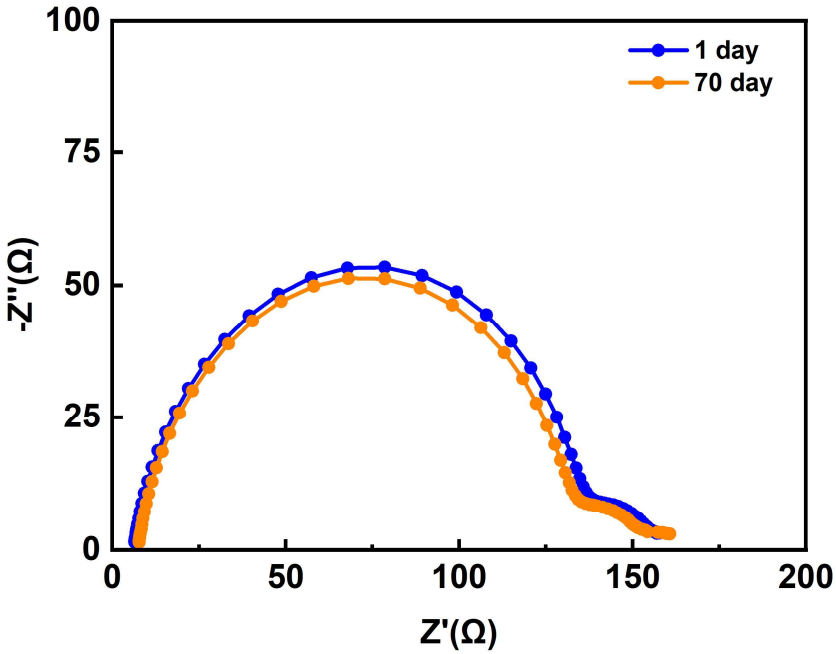

Figure S19. Time-dependent Nyquist plots of the symmetric Li cell with the SPE.

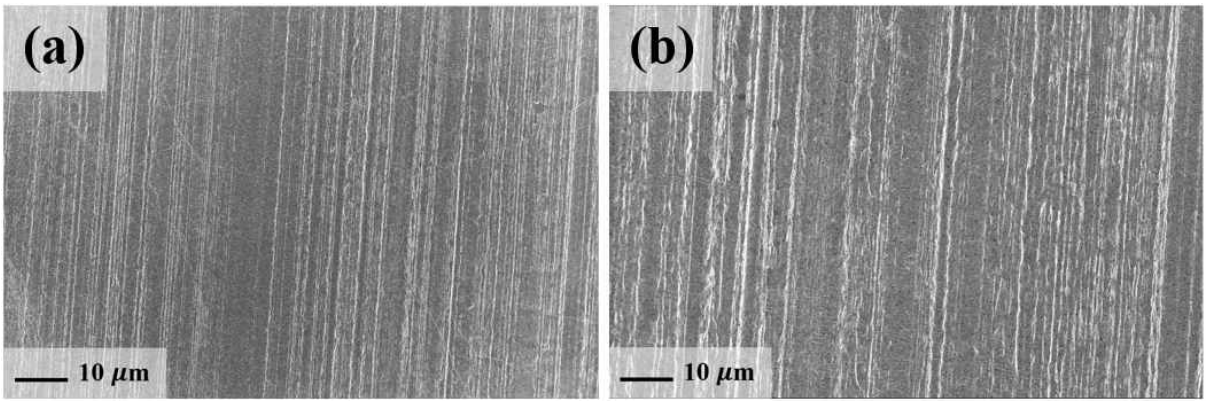

Figure S20. Top-view SEM images of the bare Li metal anodes before cycling.

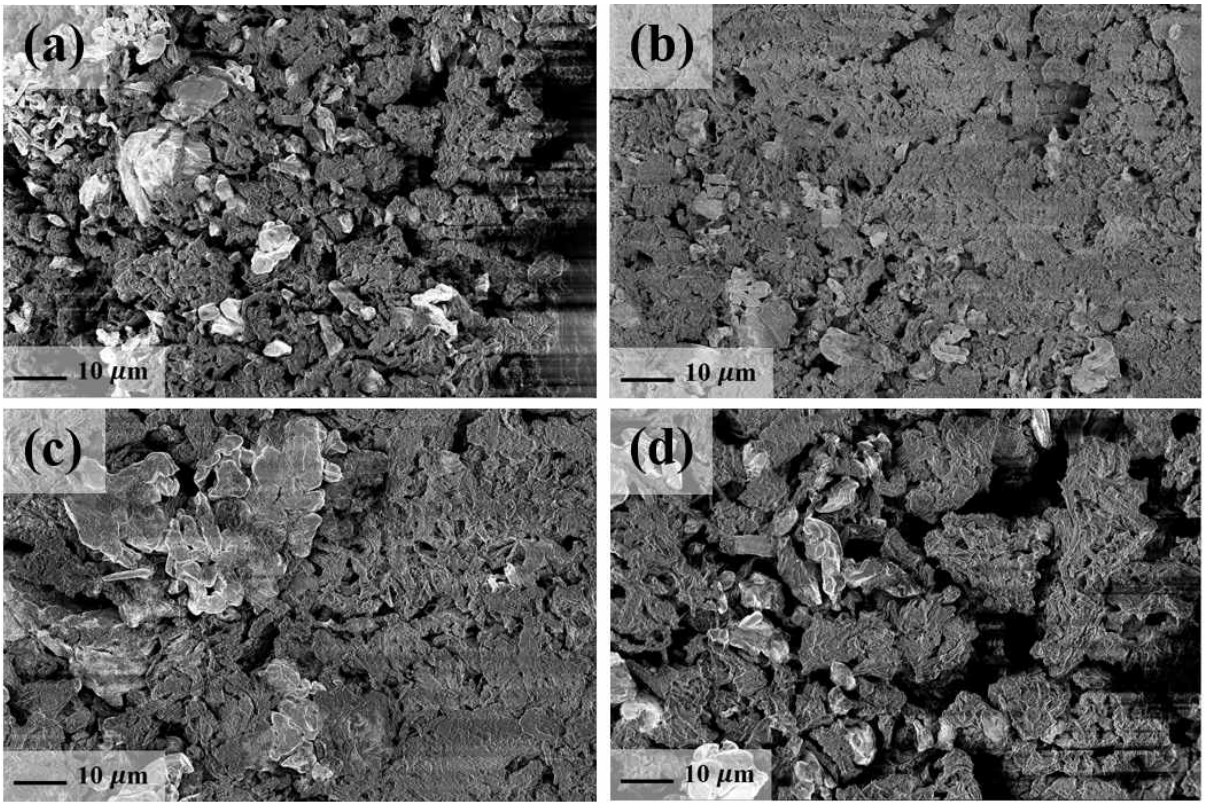

Figure S21. Top-view SEM images of the Li metal anodes after cycling with liquid electrolyte, 1.0 M $LiPF_6$ in EC/DEC (1:1 vol%) with 7.5 wt% FEC electrolyte.

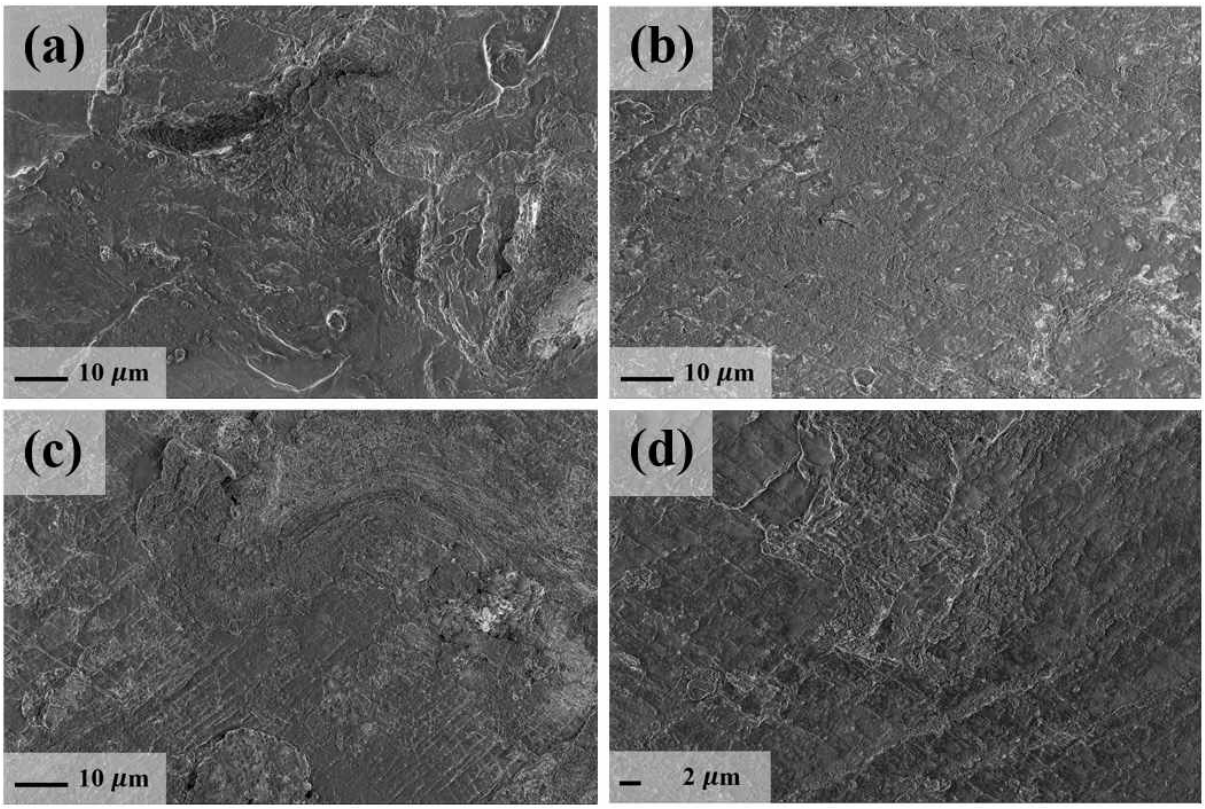

Figure S22. Top-view SEM images of the Li metal anodes after cycling with freestanding SPE.

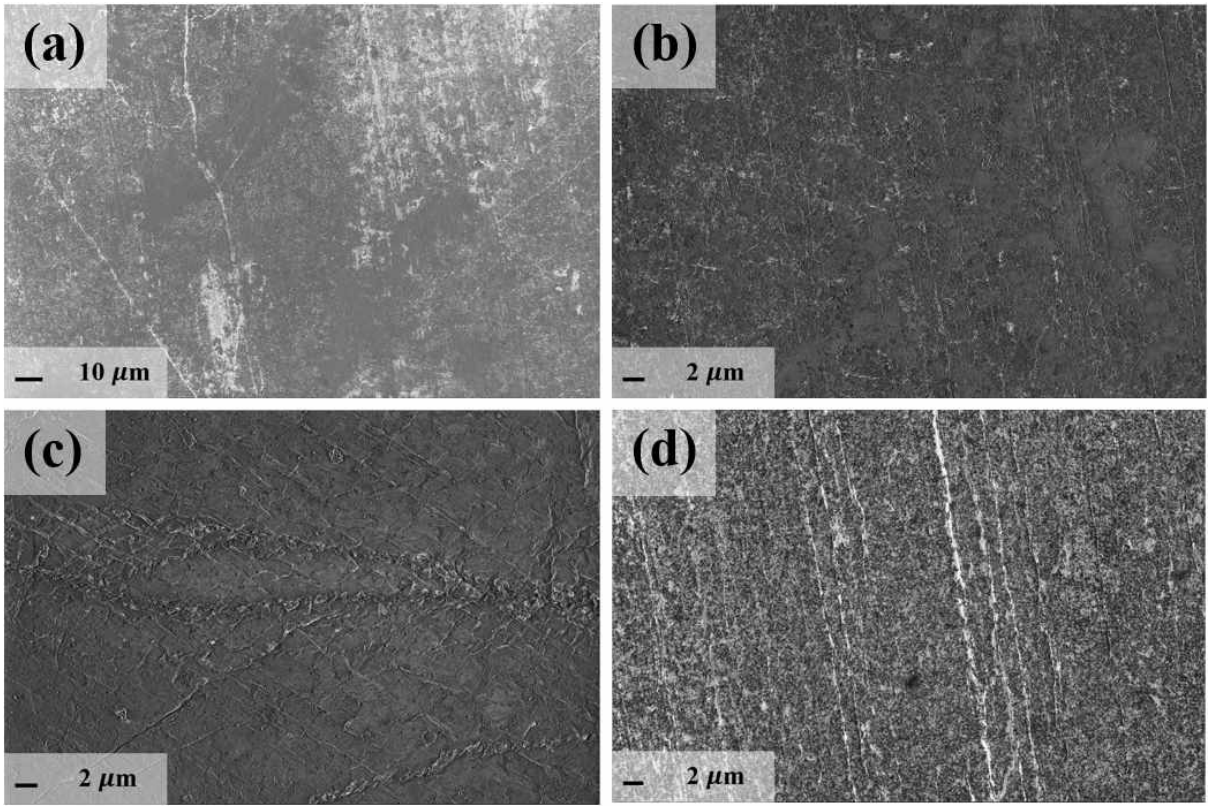

Figure S23. Top-view SEM images of the Li metal anodes after cycling with directly coated SPE.

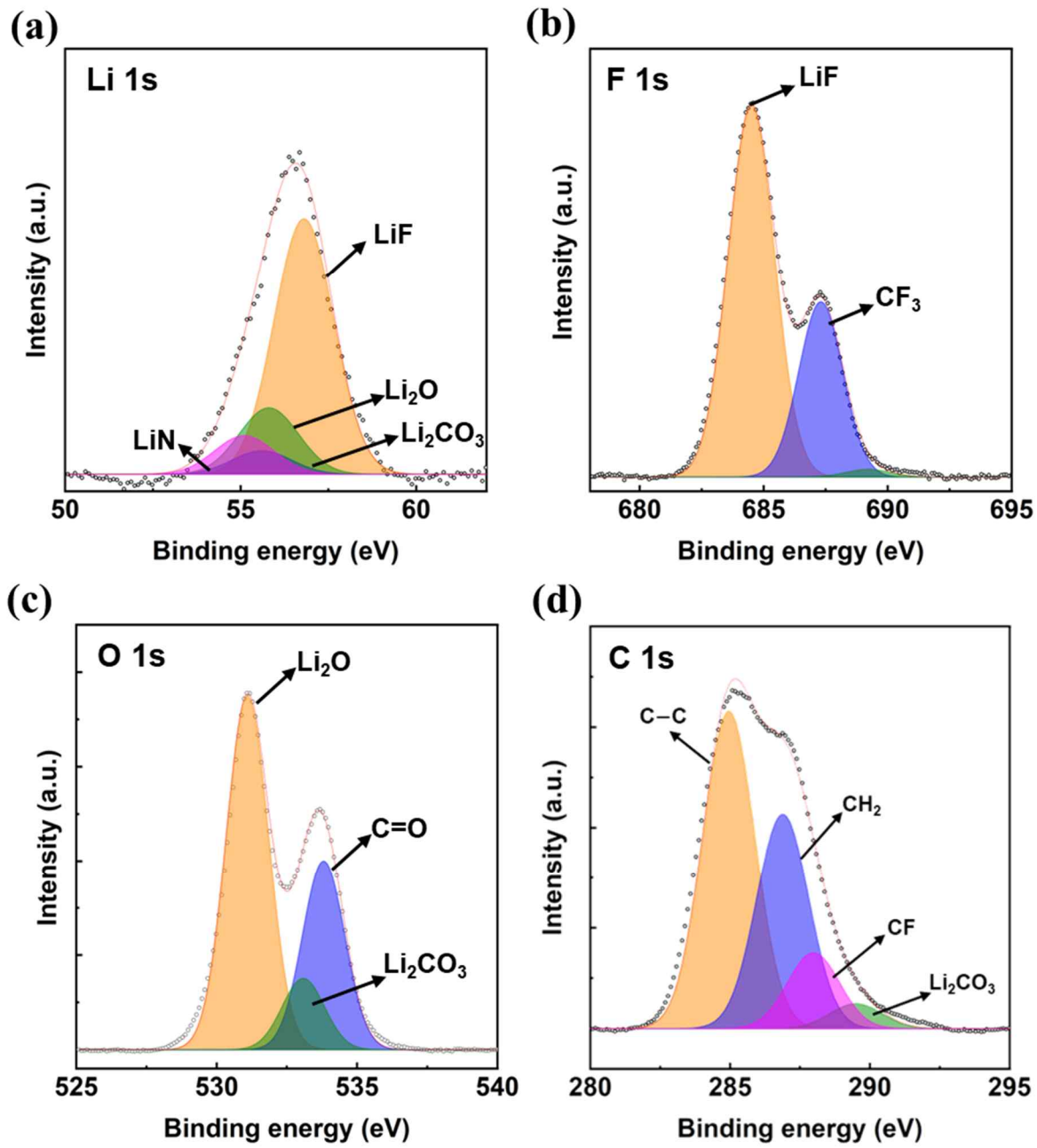

Figure S24. (a) Li 1s, (b) F 1s, (c) O 1s, and (d) C 1s XPS spectra of the Li metal anode after 100 cycles at 0.1 mA·cm^{-2} with directly coated SPE.

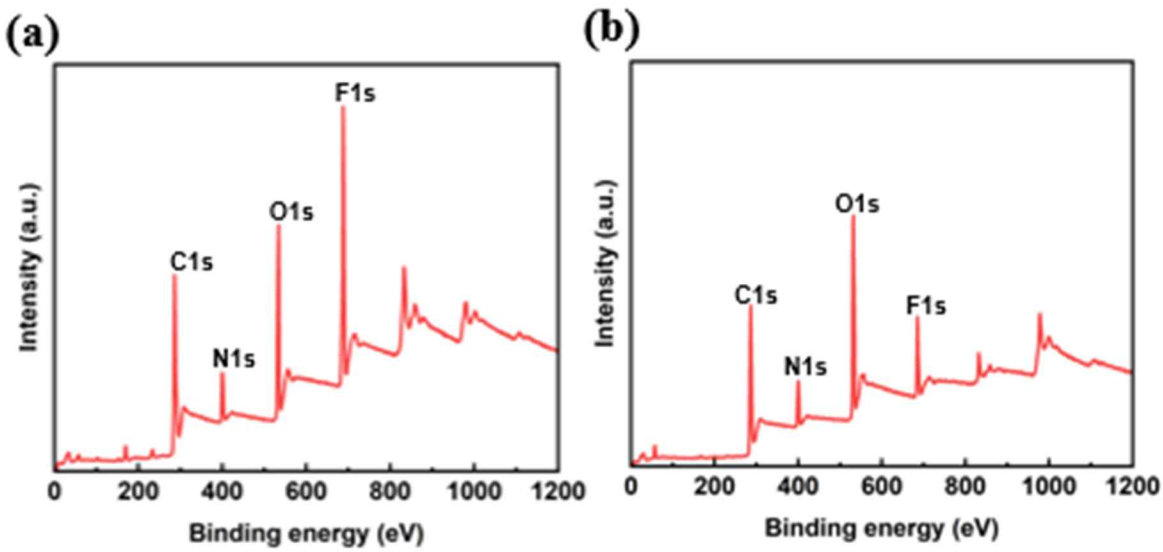

Figure S25. XPS spectra survey of the SEI after 100 cycles at 0.1 mA·cm-2 with (a) directly coated and (b) freestanding SPE.

Atomic ratio	C (%)	N (%)	O (%)	F (%)
Directly coated SPE	**49.6**	**7.9**	**18.8**	**21.2**
Freestanding SPE	52.7	8.8	32.1	5.8

Table S1. Elemental Fraction from XPS spectra survey of the SEI after 100 cycles at 0.1 mA·cm^{-2} with (a) directly coated and (b) freestanding SPE.

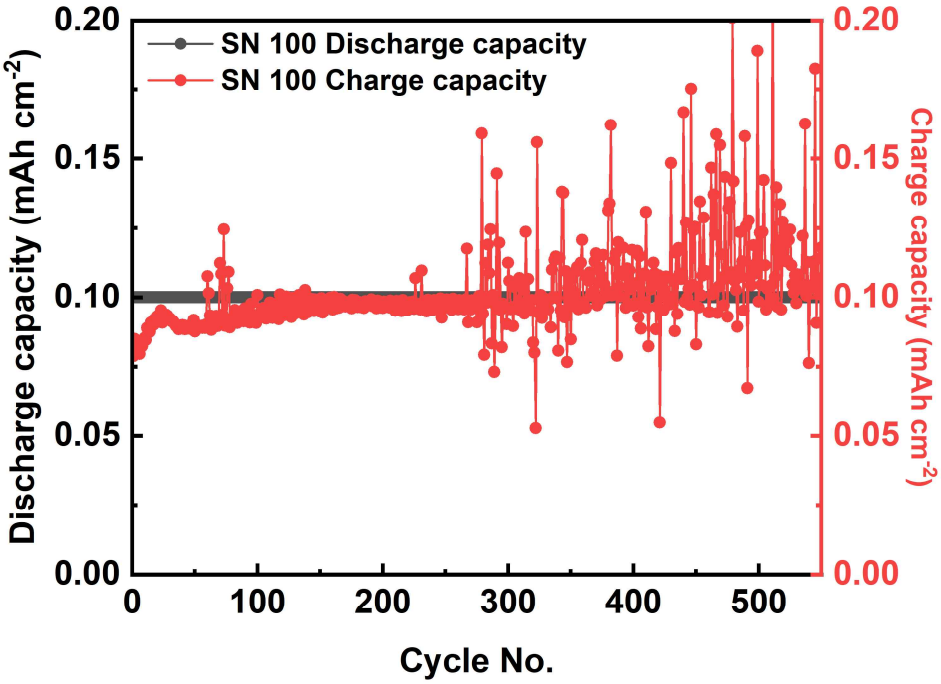

Figure S26. Cycling performance of the SN100 SPE asymmetric Li//Cu cell at a current density of 0.1 mA·cm^{-2} with a capacity of 0.1 mAh·cm^{-2}, exhibiting an overcharging phenomenon.

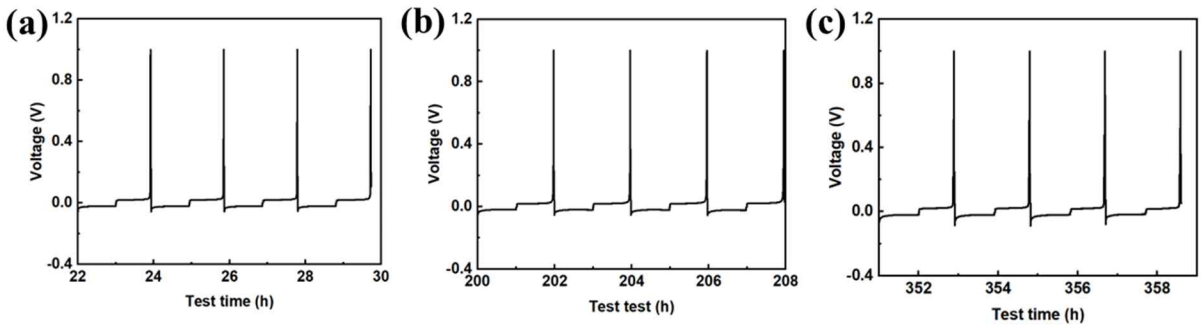

Figure S27. The cycling performance of our SPE asymmetric Li//Cu cell at current density of 0.1 mA·cm^{-2} with capacity of 0.1 mAh·cm^{-2} for different times.

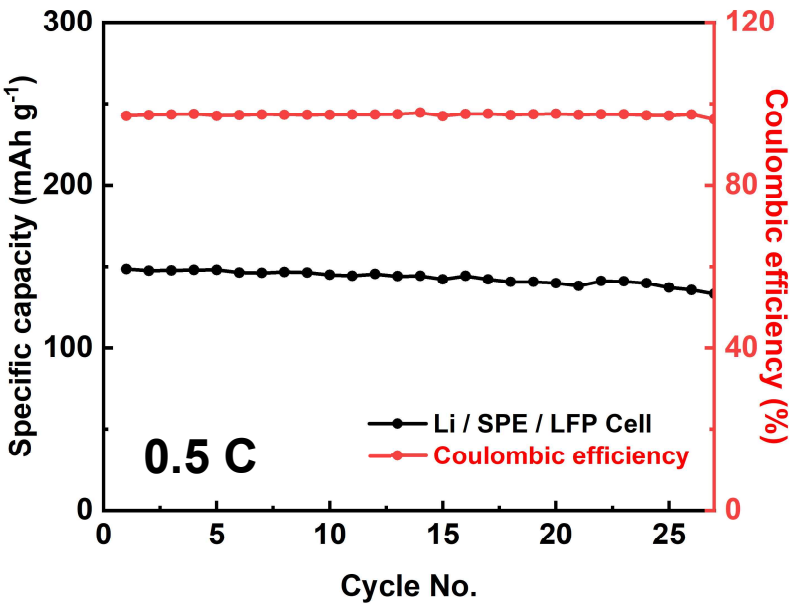

Figure S28. Cycling performance of our SPE based high-loading (4.85 mg·cm^{-2}) LFP//Li metal full cell at 0.5 C.

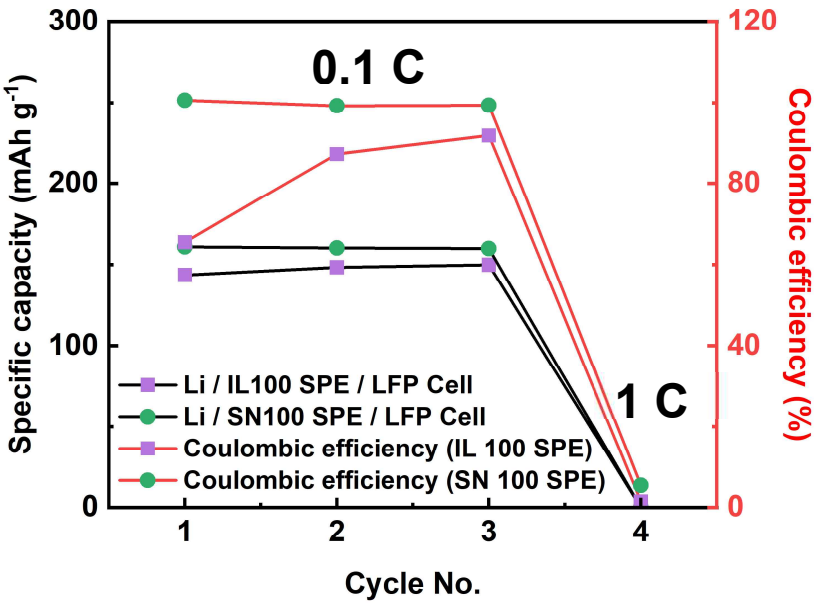

Figure S29. Cycling behavior of LFP//Li metal full cells based on IL100 and SN100 SPEs, showing failure to cycle at 1 C after initial charge-discharge at 0.1 C.

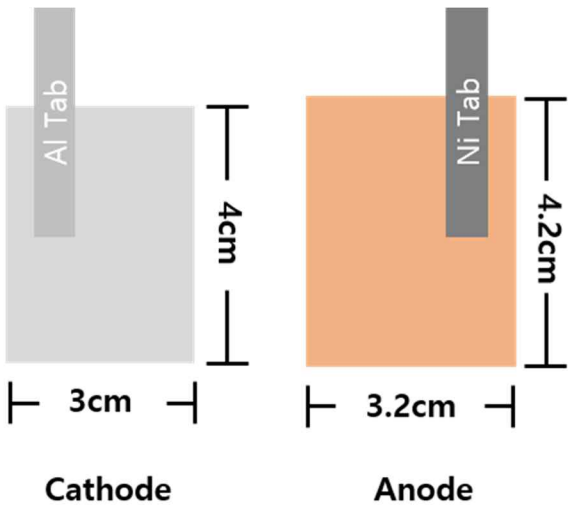

Figure S30. The Schematics and geometries of LFP, NCM Lithium metal full pouch cell.

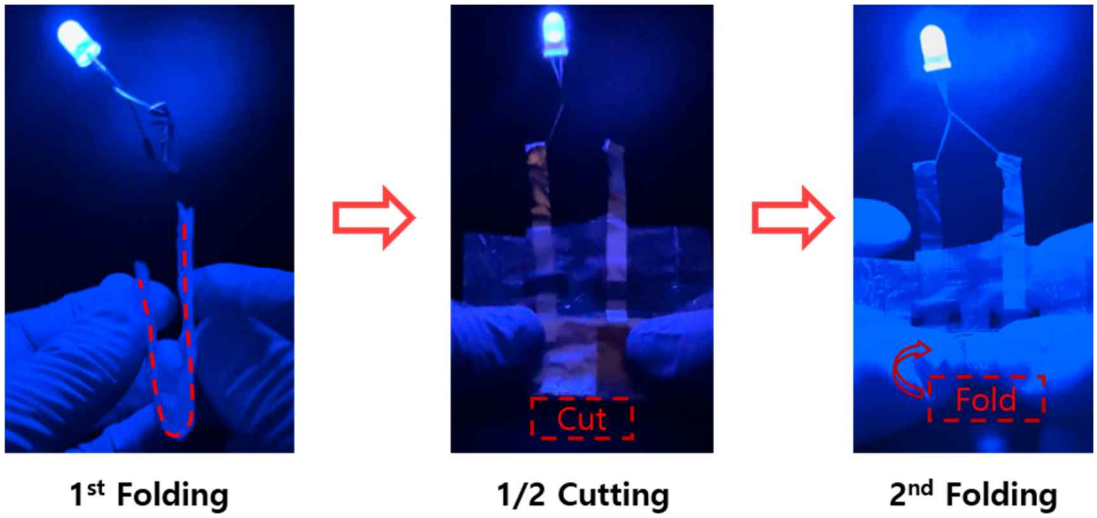

Figure S31. Folding and cutting tests of fabricated flexible pouch cells with lighting LED.

Table S2. Performance Comparison Table of Solid Polymer Electrolytes.

Polymer	SPE method	Ionic conductivity (S cm^{-1})	Li^+ transference number	Oxidation stability voltage (V)	Ref
PVDF-HFP	**UV crosslinking**	**4.7×10^{-3}**	**0.64**	**5.29**	**This work**
Butyl acrylate	Thermal crosslinking	1.1×10^{-3}	0.75	4.75	(S1)[1]
PEO, P(SSPSILi-alt-MA)	Thermal crosslinking	3.08×10^{-4}	0.97 (80 ℃)	5.0 (80 ℃)	(S2)[2]
OFHDODA	UV crosslinking	1.37×10^{-3}	0.4	5.08	(S3)[3]
PVDF-HFP	NMP(Gel)	7.24×10^{-4}	0.57	5.2	(S4)[4]
PVDF-HFP	UV crosslinking	1.03×10^{-3}	0.36	4.65	(S5)[5]
PEO	GO filler	1.54×10^{-5}	0.42 (60 ℃)	5.0 (60 ℃)	(S6)[6]

Table S3. Performance and Flexibility Comparison Table of SPE-Based Flexible Lithium Metal Batteries.

Electrolyte base	Seperator use	High C-rate (C)	Ionic conductivity (S cm^{-1})	Cathode	Cycling performance	Capacity retention (%)	Young's modulus	Bendability test (R)	Ref
PVDF-HFP	**X**	**10 C pouch cell**	**4.7×10^{-3}**	**LFP/NCM**	**2 C 150 cycles pouch cell 0.5 C 30 cycles pouch cell**	**85, 93**	**10.2 MPa**	**5 mm, (RT)**	**This work**
PEO	O	10 C coin cell (60 ℃)	3.68×10^{-5} (RT)	LFP	0.1 C 50 cycles coin cell	80.9	0.2 MPa	45°, (60 ℃)	(S7)[7]
PEGMEA/ PMMA/PS	O	7 C pouch cell (60 ℃)	1.85×10^{-5} (RT)	LFP	1 C 1000cycles pouch cell (60 ℃)	76.4	-	-	(S8)[8]
Liquid electrolyte	O	0.5 C coin cell	-	LFP	0.5 C 1000 cycles coin cell	84	-	2.5 mm	(S9)[9]
PEO	X	1 C coin cell (60 ℃)	1.54×10^{-5} (RT)	LFP	1 C 450 cycles coin cell (60 ℃)	98.7	1.31 Mpa	-	(S6)[6]
PVDF/PEI/PEG	X	3 C coin cell (60 ℃)	2.36×10^{-4} (60 ℃)	LFP	3 C 100 cycles coin cell (60 ℃)	85.9	-	-	(S10)[10]
PEGDE/PEGDA	X	0.2 C coin cell	5.3×10^{-5} (RT)	LFP	0.2 C 150cycles coin cell (55 ℃),	95.3	20.0 MPa	-	(S11)[11]
20 wt.% PBA in 5 M LiFSI/EA/TMP/FEC	O	3 C coin cell	4.2×10^{-4} (RT)	LFP	0.5 C 500 cycles coin cell	94	40.00 kPa	-	(S12)[12]

PVDF/PVAC	X	4 C coin cell	4.8×10^{-4} (RT)	LCO	0.5 C 200cycles,	85	-	-	(S13)[13]

REFERENCES

[S1] M. J. Lee, J. Han, K. Lee, Y. J. Lee, B. G. Kim, K. N. Jung, B. J. Kim, S. W. Lee, *Nature* **2022**, *601*, 217.
[S2] C. Cao, Y. Li, Y. Feng, C. Peng, Z. Li, W. Feng, *Energy Storage Mater* **2019**, *19*, 401.
[S3] L. Tang, B. Chen, Z. Zhang, C. Ma, J. Chen, Y. Huang, F. Zhang, Q. Dong, G. Xue, D. Chen, C. Hu, S. Li, Z. Liu, Y. Shen, Q. Chen, L. Chen, *Nat Commun* **2023**, *14*.
[S4] J. Jie, Y. Liu, L. Cong, B. Zhang, W. Lu, X. Zhang, J. Liu, H. Xie, L. Sun, *Journal of Energy Chemistry* **2020**, *49*, 80.
[S5] X. Wei, Y. Deng, X. Hu, Z. Yang, G. Han, H. Xu, Z. Zhang, *Chemical Engineering Journal* **2024**, *502*.
[S6] J. Wen, Q. Zhao, X. Jiang, G. Ji, R. Wang, G. Lu, J. Long, N. Hu, C. Xu, *ACS Appl Energy Mater* **2021**, *4*, 3660.
[S7] J. Wu, Z. Rao, Z. Cheng, L. Yuan, Z. Li, Y. Huang, *Adv Energy Mater* **2019**, *9*.
[S8] Z. Wang, L. Shen, S. Deng, P. Cui, X. Yao, *Advanced Materials* **2021**, *33, 2100353*.
[S9] C. Xie, J. Chang, J. Shang, L. Wang, Y. Gao, Q. Huang, Z. Zheng, *Adv Funct Mater* **2022**, *32*.
[S10] Z. Wang, J. Ma, P. Cui, X. Yao, *ACS Appl Mater Interfaces* **2022**, *14*, 34649.
[S11] H. Duan, Y. X. Yin, X. X. Zeng, J. Y. Li, J. L. Shi, Y. Shi, R. Wen, Y. G. Guo, L. J. Wan, *Energy Storage Mater* **2018**, *10*, 85.
[S12] G. Zhou, X. Lin, J. Liu, J. Yu, J. Wu, H. M. Law, Z. Wang, F. Ciucci, *Energy Storage Mater* **2021**, *34*, 629.
[S13] X. Yu, L. Wang, J. Ma, X. Sun, X. Zhou, G. Cui, *Adv Energy Mater* **2020**, *10*.